

VOLATILE-RICH CIRCUMSTELLAR GAS IN THE UNUSUAL 49 CETI DEBRIS DISK

AKI ROBERGE¹, BARRY Y. WELSH^{2,3}, INGA KAMP⁴, ALCYIA J. WEINBERGER⁵, & CAROL A. GRADY^{2,1}

Draft version October 9, 2018

ABSTRACT

We present *Hubble Space Telescope* STIS far-UV spectra of the edge-on disk around 49 Ceti, one of the very few debris disks showing sub-mm CO emission. Many atomic absorption lines are present in the spectra, most of which arise from circumstellar gas lying along the line-of-sight to the central star. We determined the line-of-sight C I column density, estimated the total carbon column density, and set limits on the O I column density. Surprisingly, no line-of-sight CO absorption was seen. We discuss possible explanations for this non-detection, and present preliminary estimates of the carbon abundances in the line-of-sight gas. The C/Fe ratio is much greater than the solar value, suggesting that 49 Cet harbors a volatile-rich gas disk similar to that of β Pictoris.

Keywords: protoplanetary disks — circumstellar matter — Kuiper belt: general — stars: individual (49 Ceti)

1. INTRODUCTION

Within about 10 Myr, gas-rich protoplanetary disks evolve into dusty, gas-poor debris disks composed of planetesimal destruction products. The details of this evolution are poorly understood, including the primary gas dissipation mechanism and the changing composition of the disk material. Disks may pass through a brief stage during which they contain both primordial material left over from star formation and secondary material from destruction of planetary bodies (e.g. Kospal et al. 2013).

The 49 Ceti disk offers a rare opportunity to explore this possibility. It is a nearby (61 pc) A1V star, recently identified as a co-moving member of the ~ 40 Myr-old Argus Association (Zuckerman & Song 2012) and long known to host a circumstellar (CS) dust disk (e.g. Sadakane & Nishida 1986). The modest amount of CS dust present led to its classification as a young debris disk. However, it is one of only three debris disks known to show sub-mm CO emission (Zuckerman et al. 1995; Dent et al. 2005; Hughes et al. 2008); the others are HD21997 (Moor et al. 2011) and β Pictoris (Dent et al. 2014). Since abundant CO gas is characteristic of a primordial or transitional disk, this led to speculation that 49 Ceti might be a rare type of protoplanetary disk just at the end of its primordial gas dissipation phase (Hughes et al. 2008). However, this identification was difficult to reconcile with the age of the system and the detection of far-IR C II emission from 49 Ceti but non-detection of O I emission (Roberge et al. 2013), which supported the suggestion that the CO gas is coming from icy comet-like bodies (Zuckerman & Song 2012).

Here we report on far-ultraviolet (FUV) absorption

spectroscopy of 49 Ceti. Since this disk is close to edge-on ($i = 90^\circ \pm 5^\circ$; Hughes et al. 2008), the line-of-sight to the central star intercepts disk material, as was shown by the detection of CS Ca II gas in optical spectra of the star (Montgomery & Welsh 2012). The FUV is rich in atomic and molecular absorption lines, permitting a much more detailed inventory of the line-of-sight CS gas, as was done in the case of β Pic (e.g. Roberge et al. 2006).

2. OBSERVATIONS

We observed 49 Ceti with the *HST* Space Telescope Imaging Spectrograph (STIS) on 2013-08-11 and 2013-08-16. FUV spectra were acquired in two visits to search for changes in CS absorption lines, since the Ca II absorption lines in 49 Ceti optical spectra showed signs of variability (Montgomery & Welsh 2012). The data were taken with E140H echelle grating and the $0''.2 \times 0''.09$ slit, providing spectra with $R = \lambda/\Delta\lambda = 228000$. In each visit, the wavelength range from 1164 Å to 1682 Å was covered using three grating settings (i1271, c1416, and c1598), with exposure times of 1663 s, 540 s, and 1878 s. The data were calibrated with the default CALSTIS v2.40 pipeline; the 1σ relative velocity accuracy within one echelle order is 0.33 km s^{-1} for the i1271 spectra and 0.16 km s^{-1} for the c1416 and c1598 spectra⁶. The absolute wavelength accuracy between echelle orders is 0.66 km s^{-1} for the i1271 spectra and 0.33 km s^{-1} for the c1416 and c1598 spectra.

We detected narrow absorption lines arising from the following species: C I, C II, C IV, O I, Cl I, S I, Si II, Al II, and Fe II. Lines arising from excited fine-structure energy levels, which are not seen in spectra of the local interstellar (IS) medium, are present. The wings of strong lines arising from abundant ionized species (C II and C IV) showed significant variable absorption, indicating transient gas falling toward the central star at high velocity. These features greatly resemble those seen in FUV spectra of β Pic (e.g. Roberge et al. 2000; Bouret et al. 2002) and likely arise from the same phenomenon – tran-

¹ Exoplanets & Stellar Astrophysics Laboratory, NASA Goddard Space Flight Center, Code 667, Greenbelt, MD 20771, USA

² Eureka Scientific, 2452 Delmer, Suite 100, Oakland, CA 96002, USA

³ Space Sciences Laboratory, University of California, 7 Gauss Way, Berkeley, CA 94720, USA

⁴ Kapteyn Astronomical Institute, University of Groningen, 9700 AV Groningen, Netherlands

⁵ Department of Terrestrial Magnetism, Carnegie Institution for Science, 5241 Broad Branch Road NW, Washington, DC 20015, USA

⁶ STIS Instrument Handbook, V13.0:
<http://www.stsci.edu/hst/stis/documents/handbooks/currentIHB/cover.htm>

sits of star-grazing planetesimals (e.g. Beust et al. 1990). Analysis of the variable features will be presented in a future paper. No emission lines were seen, except Lyman α emission very likely coming from terrestrial airglow. This shows that the central star is chromospherically inactive.

3. CIRCUMSTELLAR CARBON

3.1. Spin-forbidden C I 1613.4 Å line

The spin-forbidden C I absorption line at 1613.4 Å, arising from the ground energy level of C I (3P_0), appears in the spectra from both visits. This weak line remains unsaturated to high abundances, making it valuable for accurate measurements of large column densities (e.g. Roberge et al. 2000). There is no hint of variability or multiple absorption components at different velocities. Therefore, the spectra from the two visits were averaged together to increase the S/N (Figure 1). To correct for any wavelength shift between the two exposures, the data were aligned before averaging by cross-correlating over a small wavelength region near the line. The 1613.4 Å line is detected at the 5σ level. The two lines in the triplet arising from the 1st and 2nd excited fine structure energy levels (C I* at 1613.8 and C I** 1614.5 Å) were not detected.

The continuum around the line was fit with a 4th-degree polynomial and the spectrum normalized. We then measured the equivalent width (EQW) of the line and the column density in the ground energy level, $N(^3P_0) = (2.66 \pm 0.51) \times 10^{15} \text{ cm}^{-2}$. This is about 44% of the line-of-sight C I 3P_0 column density towards β Pic (Roberge et al. 2000). The line was fit with a Gaussian to determine the heliocentric velocity of the gas and the Doppler broadening parameter, $b = 1.32 \pm 0.35 \text{ km s}^{-1}$; the error is the statistical uncertainty added in quadrature with the uncertainty in the relative calibration of the wavelength scale⁶.

The velocity is $v_{\text{CI}} = 11.59 \pm 0.40 \text{ km s}^{-1}$, where the error includes the uncertainty in the absolute wavelength calibration⁶. The velocity is close to the radial velocity of the central star ($v_* = 12.2 \text{ km s}^{-1}$; Hughes et al. 2008). Unfortunately, the star's velocity is also close to the velocity of the local IS cloud in the direction of 49 Cet ($v_{\text{LIC}} = 11.0 \pm 1.3 \text{ km s}^{-1}$; Redfield & Linsky 2008). This makes it impossible to identify the C I absorption as being purely CS on the basis of velocity alone. However, the favored ionization state for carbon in the diffuse ISM is C II and local IS C I abundances are very low ($N(^3P_0) \lesssim 10^{12} \text{ cm}^{-2}$; Welsh & Lallement 2010). Therefore, this large amount of C I gas towards 49 Cet is likely to be almost entirely CS.

3.2. C I 1560 Å multiplet

Several strong dipole-allowed multiplets of C I are visible in the spectra; the multiplet that lies in a region of the spectrum with the highest continuum S/N is at 1560 Å (Figure 2). Lines arising from the first three fine structure energy levels are clearly detected, so we are able to constrain the excitation temperature and the total column density. The C I 1560 Å multiplet did not vary significantly between the two visits, and there are no obvious signs of multiple velocity components. Therefore, the spectra from the two visits were aligned in wavelength, then averaged together to increase the S/N .

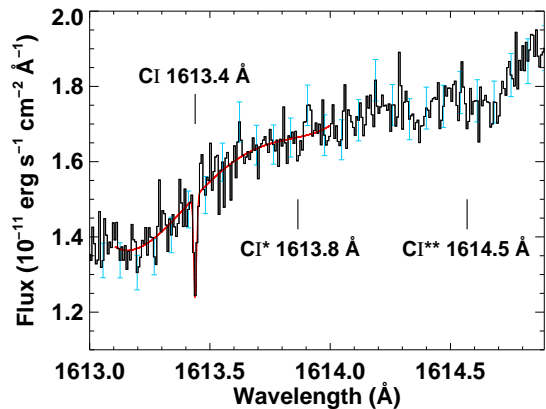


Figure 1. The spin-forbidden C I 1613 Å triplet in the averaged 49 Cet spectrum. Flux error bars are shown in light blue. The red line shows the continuum model for the region around the 1613.4 Å line, with the best-fitting Gaussian model for the absorption line superimposed. The two lines arising from excited fine-structure energy levels were not detected.

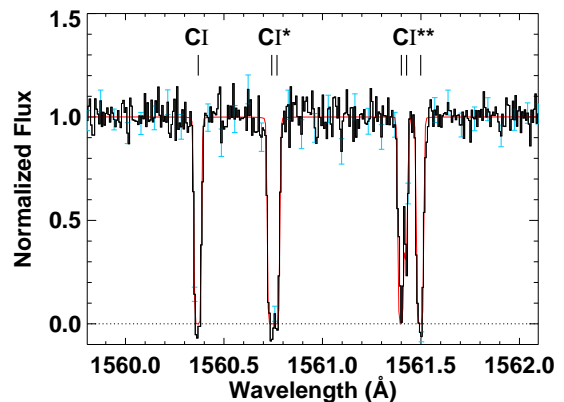


Figure 2. The strong dipole-allowed C I 1560 Å multiplet in the averaged, normalized 49 Cet spectrum. The red line shows the best-fitting absorption model.

We created models of the multiplet containing a single velocity component, assuming LTE for the population of the fine structure levels, and using Voigt line profiles appropriate for saturated lines. The free parameters in the models are the total column density in the 3P ground term ($N(^3P)$), the excitation temperature (T_{ex}), b , and v . The best parameters were found by χ^2 minimization, varying all free parameters over large ranges of parameter space. The uncertainties on the best parameters were determined by projecting the χ^2 contours, which were well-behaved with only a single minimum seen. The total column density is $N(^3P) = 4.47^{+1.15}_{-0.43} \times 10^{15} \text{ cm}^{-2}$, which is within the upper limit on the total column density determined from the non-detections of the excited lines in the 1613 Å triplet. The excitation temperature is $T_{\text{ex}} = 38.0^{+8.0}_{-3.8} \text{ K}$. The Doppler broadening parameter is $b = 1.65 \pm 0.17 \text{ km s}^{-1}$ and the velocity is $v = 11.00 \pm 0.33 \text{ km s}^{-1}$, which agrees with the velocity determined from the 1613.4 Å line within the errors.

3.3. Total carbon

A strong saturated doublet arising from C II at 1334 Å is seen in the data. Ideally, measurement of the CS

C II column density would allow us to calculate the total abundance of CS carbon along the line-of-sight to 49 Cet. Unfortunately, the line arising from the ground energy level will contain blended IS contamination. Furthermore, both C II features varied between the two visits, showing that some of the gas likely arises from star-grazing planetesimals. Modeling of these lines will be very difficult and is deferred to a later paper.

To roughly estimate the total CS carbon column density, we make use of elemental neutral fractions calculated for a similar environment, the disk around the A5V star β Pic. Ionization balance calculations indicated that the β Pic carbon gas is about 60% neutral (Fernandez et al. 2006), which was confirmed by observation (Roberge et al. 2006). The β Pic and 49 Cet central stars are both A-type and their disks have a similar total dust abundance (based on their fractional dust luminosities). While sub-mm observations suggest that the 49 Cet disk as a whole contains more CO than β Pic (Hughes et al. 2008; Dent et al. 2014), the two CS environments appear otherwise similar. Fernandez et al. (2006) also provided calculated neutral fractions for β Pic-like gas disks with different central stars. For an A0V star (close to the A1V spectral type of 49 Cet), the carbon neutral fraction should be about 1%, giving a total CS carbon column density along the line-of-sight of $\sim 4.5 \times 10^{17} \text{ cm}^{-2}$.

4. CIRCUMSTELLAR OXYGEN

Three lines of O I at 1302.2, 1304.9, and 1306.0 Å were seen in the spectra (Figure 3), arising from the three fine structure energy levels of the ground term (3P_2 , 3P_1 , and 3P_0). The line arising from the ground level is very likely contaminated with blended IS absorption; furthermore, there appears to be an additional blueshifted component in the absorption. While there was no *significant* variation in the blueshifted feature between the two visits, there is a hint that it changed in depth, indicating that it is likely due to a star-grazing comet. The complexity, strength, and relatively low S/N of the O I 1302.2 Å absorption feature make it challenging to model.

However, the O I* and O I** lines arising from the excited levels come solely from CS gas, since the column density of O I* in the local ISM is $\lesssim 2 \times 10^{12} \text{ cm}^{-2}$ (Welsh & Lallement 2010). These lines did not vary significantly between the two visits and there are no obvious signs of multiple velocity components. We modeled these lines first, to illuminate the velocity structure of the CS O I component and then use that information to aid modeling of the saturated, blended O I 1302.2 Å line.

For the O I* and O I** lines, we performed a χ^2 minimization analysis similar to the one described for the C I 1560 Å multiplet. Models for the two lines were created with a single velocity component. One difference is that we did not assume LTE for these models. Unlike C I, the separations between the fine structure energy levels of O I are large and very high temperature and density are required for O I gas to be in LTE. The free parameters in the models are $N(^3P_1)$, $N(^3P_0)$, b , and v . Again, the contours of χ^2 were well-behaved with only a single minimum seen. We found $N(^3P_1) = (7.08 \pm 0.92) \times 10^{13} \text{ cm}^{-2}$, $N(^3P_0) = (3.16 \pm 0.91) \times 10^{13} \text{ cm}^{-2}$, $b = 1.75 \pm 0.34 \text{ km s}^{-1}$, and $v = 12.6 \pm 0.70 \text{ km s}^{-1}$.

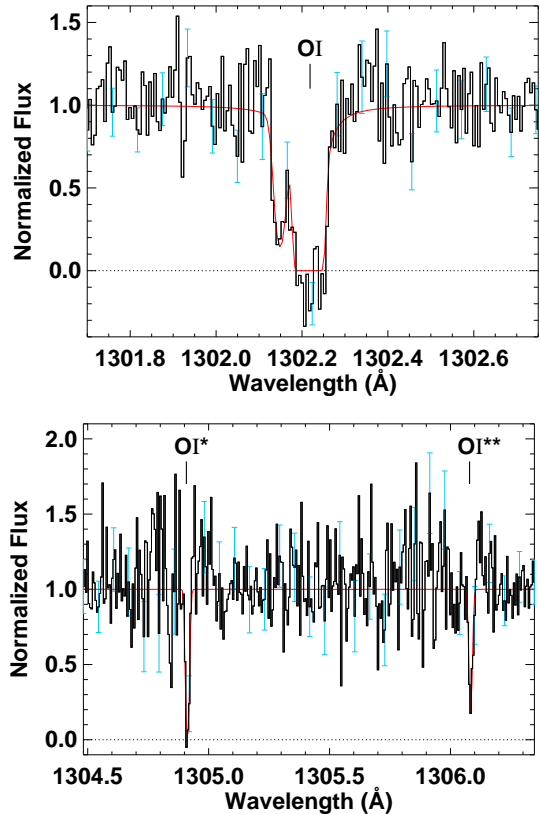


Figure 3. The O I 1302 Å multiplet in the averaged, normalized 49 Cet spectrum. The top panel shows the saturated, blended O I line at 1302.2 Å, while the bottom panel shows the weaker O I* and O I** lines arising purely from CS gas. The red lines show the best-fitting absorption models.

The velocity of the gas agrees very well with the velocity of 49 Cet (12.2 km s^{-1}), consistent with a gas disk in Keplerian rotation about the star.

We then created models of the O I 1302.2 Å line with three velocity components: a CS component with the b and v values determined from the O I* and O I** lines, an IS component at the velocity of the local IS cloud toward 49 Cet (11 km s^{-1} ; Redfield & Linsky 2008) and the mean b value for O I in the local ISM (3.24 km s^{-1} ; Redfield & Linsky 2004), and a blueshifted component. The free parameters in the models were $N_{\text{CS}}(^3P_2)$, $N_{\text{IS}}(^3P_2)$, $N_{\text{BS}}(^3P_2)$, b_{BS} , and v_{BS} . As before, χ^2 minimization was performed over large ranges of parameter space; the best-fitting model appears in Figure 3. However, the χ^2 contours were not well-behaved this time, with signs of multiple minima and open-ended contours for $N_{\text{CS}}(^3P_2)$. This indicates that the modeling is too degenerate to draw strong conclusions about the best parameters.

However, we were able to set a 3σ lower limit on the *combined* IS/CS column density, $N_{\text{IS/CS}}(^3P_2) \gtrsim 2 \times 10^{16} \text{ cm}^{-2}$. We could also set a 3σ upper limit on $N_{\text{CS}}(^3P_2) \lesssim 1 \times 10^{17} \text{ cm}^{-2}$. The upper limit on $N_{\text{CS}}(^3P_2)$ that we calculated from non-detection of a weak spin-forbidden O I line at 1355.6 Å is similar ($\leq 1.85 \times 10^{17} \text{ cm}^{-2}$).

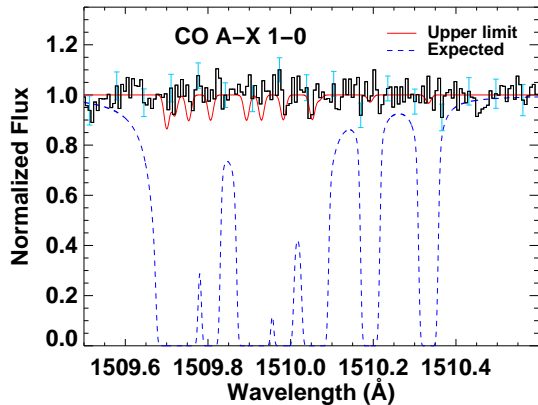


Figure 4. Non-detection of line-of-sight CO absorption. The black line shows the averaged, normalized spectrum in the region of the $A - X$ (1-0) band. The red line is a model for the absorption band with the 3σ upper limit on the column density in each rotational level. The blue dashed line is a model for the expected absorption based on analysis of the observed sub-mm CO emission from 49 Cet (Hughes et al. 2008).

5. UPPER LIMIT ON CARBON MONOXIDE

No absorption was seen in any of the bands of the CO fourth positive system ($A^1\Pi - X^1\Sigma^+$). Figure 4 shows the region around the $A - X$ (1-0) band. To calculate upper limits on CO in the five lowest rotational levels ($J_l = 0 - 4$), we fit the continua in the regions of the (0-0), (1-0), (2-0), and (3-0) bands with polynomials, then normalized the spectra. The EQW and error was calculated for every line arising from the $J_l = 0, 1, 2, 3$, and 4 levels, then converted into a column density and uncertainty. For each rotational level, the line with the smallest EQW uncertainty was used to set the 3σ upper limit on the column density (Table 1).

The non-detection of CO absorption in these spectra was surprising, given the edge-on inclination of the 49 Cet disk observed in emission with the Submillimeter Array ($i = 90^\circ \pm 5^\circ$; Hughes et al. 2008). Based on models of the observed sub-mm CO emission in Hughes et al. (2008), we expected a CO excitation temperature of 250 K and a line-of-sight column density of $2.8 \times 10^{18} \text{ cm}^{-2}$, which is about 5 orders of magnitude above our 3σ upper limit on the total line-of-sight absorption. A model of the expected absorption in the CO (1-0) band appears in Figure 4.

6. DISCUSSION

6.1. Why is C absorption seen, but no CO?

First, for there to be bright sub-mm CO emission from 49 Cet but no line-of-sight CO absorption, the molecular gas disk must not be as edge-on as was thought. This will be confirmed or denied by a new high spatial resolution CO map of 49 Cet obtained with ALMA (Hughes et al., in preparation). Once the true inclination of the 49 Cet molecular gas disk is established, the lack of line-of-sight CO will provide a strong constraint on the scale height of the gas.

Second, the detection of C and O absorption along the line-of-sight to the central star but non-detection of CO absorption shows that the spatial distributions of atomic and molecular gas in this disk are different. The atomic absorption lines contain a component close to the velocity of the central star, which does not significantly vary

Table 1
 3σ upper limits on line-of-sight CO absorption

Lower level	Column density (cm^{-2})
$J = 0$	$\leq 2.9 \times 10^{12}$
$J = 1$	$\leq 5.8 \times 10^{12}$
$J = 2$	$\leq 5.6 \times 10^{12}$
$J = 3$	$\leq 5.4 \times 10^{12}$
$J = 4$	$\leq 5.2 \times 10^{12}$
Total	$\leq 2.5 \times 10^{13}$

between the two days of observation. This component greatly resembles the so-called “stable” component seen in spectra of β Pic, which is associated with a gas disk in Keplerian rotation about the star (e.g. Lagrange et al. 1998). It appears likely that 49 Cet too has a stable component.

Such a stable component could arise in a largely atomic gas disk rotating about the star, as with β Pic. This disk would have to have a larger scale height than the molecular disk, which could happen if much of the atomic gas is produced from comets with a wide range of inclinations. But given the presence of abundant CO, one must also consider the possibility that the atomic gas is a dissociated and ionized skin over the molecular gas disk. Hopefully, ALMA maps of CO emission (recently acquired) and C I fine structure emission (upcoming in Cycle 2) will reveal the spatial distributions of molecular and atomic gas in the disk.

6.2. Preliminary carbon abundances in the CS gas

Given its high first ionization energy, the bulk of the oxygen should be in the neutral state. Therefore, the upper limit on the total line-of-sight CS oxygen column density is $N_O \lesssim 10^{17} \text{ cm}^{-2}$. The approximate C/O number ratio is then $\gtrsim 4.5$, which is about 9 times greater than the solar C/O ratio (0.5; Lodders 2003). This value should be taken with a grain of salt, however, since we only estimated the CS C II column density. It needs to be confirmed, if possible, by modeling the complex, saturated, and variable C II absorption features in our spectra.

Malamut et al. (2014) analyzed two strong near-UV Fe II absorption lines towards 49 Cet and found two velocity components, one IS and one CS. The CS component had $v = 13.65 \pm 0.15 \text{ km s}^{-1}$, $b = 2.50 \pm 0.28 \text{ km s}^{-1}$, and $N = 1.86^{+0.48}_{-0.38} \times 10^{13} \text{ cm}^{-2}$. The neutral fraction for Fe II around 49 Cet should be 3×10^{-6} , assuming a β Pic-like gas disk around an A0V star (Fernandez et al. 2006). This is supported by non-detection of an Fe I line at 3859.9 Å in optical spectra of 49 Cet (Welsh & Montgomery, in preparation). So nearly all the Fe should be in the 1st ionized state and the total column density of CS iron is $1.86 \times 10^{13} \text{ cm}^{-2}$.

Therefore, the C/Fe number ratio in the line-of-sight CS gas is ~ 24000 . The solar C/Fe number ratio is 8.7 (Lodders 2003), so the CS carbon along the line-of-sight to 49 Cet appears to be overabundant by a factor of about 2800. Even if we ignore C II and take the reliable C I column density to be the total carbon column density, the C/Fe ratio is still ~ 28 times the solar value.

An extreme carbon overabundance relative to iron,

together with a more normal C/O ratio, is also seen in the β Pic CS gas (Roberge et al. 2006; Xie et al. 2013). Both gas disks appear to be volatile-rich. For a long time, it was not understood why radiation pressure does not rapidly blow away much of the β Pic CS gas (Lagrange et al. 1998). Fernandez et al. (2006) showed that the moderately ionized β Pic gas couples into a single ionic fluid with an effective radiation pressure coefficient, and that a carbon overabundance lowers the coefficient, keeping the whole gas disk bound to the star. The carbon overabundance now seen in 49 Cet may play a similar role.

In this scenario, small velocity shifts between different atomic species are expected, as neutral species may be slightly accelerated by radiation pressure before being ionized and joining the ionic fluid. This may explain why the CS C I velocity we measured is slightly blueshifted with respect to the CS Fe II velocity measured by Malamut et al. (2014). Detailed calculations of the 49 Cet gas dynamics and comparison to the exact radial velocities of the observed species will provide a strong test of this theory.

Support for program number GO-12901 was provided by NASA through a grant from the Space Telescope Science Institute, which is operated by the Association of Universities for Research in Astronomy, Inc., under NASA contract NAS5-26555. A. R. also acknowledges support by the Goddard Center for Astrobiology, part of the NASA Astrobiology Institute.

Facilities: HST (STIS).

REFERENCES

- Beust, H., Vidal-Madjar, A., Ferlet, R., & Lagrange-Henri, A. M. 1990, *A&A*, 236, 202
- Bouret, J.-C., Deleuil, M., Lanz, T., et al. 2002, *A&A*, 390, 1049
- Dent, W. R. F., Greaves, J. S., & Coulson, I. M. 2005, *MNRAS*, 359, 663
- Dent, W. R. F., Wyatt, M. C., Roberge, A., et al. 2014, *Science*, 343, 1490
- Fernandez, R., Brandeker, A., & Wu, Y. 2006, *ApJ*, 643, 509
- Hughes, A. M., Wilner, D. J., Kamp, I., & Hogerheijde, M. R. 2008, *ApJ*, 681, 626
- Kospal, A., Moor, A., Juhasz, A., et al. 2013, *ApJ*, 776, 77
- Lagrange, A.-M., Beust, H., Mouillet, D., et al. 1998, *A&A*, 330, 1091
- Lodders, K. 2003, *ApJ*, 591, 1220
- Malamut, C., Redfield, S., Linsky, J. L., Wood, B. E., & Ayres, T. R. 2014, *ApJ*, 787, 75
- Montgomery, S. L., & Welsh, B. Y. 2012, *PASP*, 124, 1042
- Moor, A., Abraham, P., Juhasz, A., et al. 2011, *ApJ*, 740, L7
- Redfield, S., & Linsky, J. L. 2004, *ApJ*, 602, 776
- . 2008, *ApJ*, 673, 283
- Roberge, A., Feldman, P. D., Lagrange, A. M., et al. 2000, *ApJ*, 538, 904
- Roberge, A., Feldman, P. D., Weinberger, A. J., Deleuil, M., & Bouret, J.-C. 2006, *Nature*, 441, 724
- Roberge, A., Kamp, I., Montesinos, B., et al. 2013, *ApJ*, 771, 69
- Sadakane, K., & Nishida, M. 1986, *PASP*, 98, 685
- Welsh, B. Y., & Lallement, R. 2010, *PASP*, 122, 1320
- Xie, J.-W., Brandeker, A., & Wu, Y. 2013, *ApJ*, 762, 114
- Zuckerman, B., Forveille, T., & Kastner, J. H. 1995, *Nature*, 373, 494
- Zuckerman, B., & Song, I. 2012, *ApJ*, 758, 77